Professional paper

Received: June 5, 2013
Accepted: November 20, 2013

Hydro-geophysical evaluation of groundwater potential in hard rock terrain of southwestern Nigeria

Hidrološko-geofizikalna opredelitev potenciala podtalnice v ozemlju trdnih kamnin v jugozahodni Nigeriji

Ayodeji Jayeoba*, Michael Adeyinka Oladunjoye
University of Ibadan, Department of Geology, Ibadan, Nigeria
*Corresponding author. E-mail: a.jayeoba@mail.ui.edu.ng

Abstract

In an attempt to characterize groundwater potential at the recently acquired land for University of Ibadan Cooperative Housing Estate located at Alabata near Ibadan, South-western Nigeria, integrated geophysical survey involving Very Low Frequency-Electromagnetic (VLF-EM) and resistivity methods were adopted. The VLF data measured along eight profiles were processed applying Fraser filtering and Karous-Hjelt filter on measured real components of the field data. Structural features significant to groundwater development were evident in the Fraser filter map and equivalent current density pseudo-sections. Thirteen Vertical Electrical soundings (VES) were carried out across the area using the Schlumberger electrode array configuration, with half-current electrode separation (AB/2) varying from 1 m to 100 m. The layer model interpretation obtained from the sounding curves revealed three to four layer earth models categorized into topsoil, lateritic hardpan, partially weathered layer and the fresh bedrock. The overburden thickness varies from 4.9 m to 19.1 m. Maps of the aquifer resistivity, aquifer thickness, overburden thickness, basement relief, bedrock resistivity, and secondary geoelectric (Dar-Zarrouk) parameters revealed delineated area with prolific aquiferous groundwater potentials.

Key words: Alabata area, geophysical investigation, current density map, geo-electric map, prolific zones.

Izvleček

Pri poskusu opredelitve potenciala podtalnice v zemljišču, nedavno nabavljenem za zadružno stanovanjsko gradnjo pri Ibadanski univerzi v Alabati pri Ibadanu v jugozahodni Nigeriji, so izvedli integrirano geofizikalno raziskavo, pri kateri so uporabili zelo nizkofrekvenčno elektromagnetno (Very Low Frequency-Electromagnetic -VLF-EM) in upornostno metodo. Podatke VLF-merjenj v osmih profilih so obdelali z uporabo Fraserjevega filtriranja in Karous-Hjeltovega filtra na merjenih realnih komponentah terenskih podatkov. Strukturne značilnosti, povezane s prisotnostjo podtalnice, so se pokazale na kartah Fraserjevega filtriranja in psevdopreseki ekvivalentne tokovne gostote. Na preiskovanem območju so izvedli trinajst vertikalnih električnih sondiranj (VES) po Schlumbergerovem razporedu elektrod s polovičnim razmikom tokovnih elektrod (AB/2) od 1 m do 100 m. Z interpretacijo plastovnega modela, dobljenega iz krivulj sondiranja, so postavili model treh do štirih plasti, ki ustrezajo tlom, trdni lateritni plasti, plasti delne preperine in neprepereli matični kamnini. Debelina krovnih plasti je od 4,9 m do 19,1 m. Iz kart upornosti v vodonosniku, njegove debeline, debeline krovnih plasti, reliefa podlage, upornosti podlage in sekundarnih geoelektričnih lastnosti (Dar-Zarrouk) je bilo mogoče določiti območja obetavne izdatnosti podtalnice.

Ključne besede: območje Alabata, geofizikalna raziskava, karta tokovne gostote, geoelektrična karta, cone izdatnosti

Introduction

University of Ibadan cooperative recently acquired a parcel of land to serve as housing estate for its members. The basement complex rocks of southwestern Nigeria underlie the estate, which is located at Alabata near Ibadan. In typical hard rock areas, the geological sequence normally encountered is characterized by the existence of basement rock overlain by variable unconsolidated materials referred to as overburden. The groundwater in a typical Basement Complex environment is usually contained in the weathered and/or fractured basement rocks or alluvial deposits within flood plains.[1] However, the discontinuous nature of the basement aquifer system makes detailed knowledge of the subsurface geology, its weathering depth and structural disposition through geologic and geophysical investigations inevitable.[2] In order to evolve a pragmatic and scientific planning for the management of groundwater resources in this estate, a hydro-geophysical evaluation of the groundwater potential was carefully carried out.

Integrated geophysical tools, especially resistivity and electromagnetic methods, are commonly used in groundwater exploration, mainly due to the close relationship between electrical conductivity and some hydrological parameters. The Very Low Frequency Electromagnetic (VLF-EM) is an effective tool in mapping conductive fault and fracture zones while resistivity method is used for detecting groundwater presence and differentiating subsurface layers. Electrical and electromagnetic geophysical methods have been widely used in groundwater investigations because of good correlation between electrical properties, geological (composition) and fluid content.[3–6] In present paper, Very Low Frequency (VLF-EM) and Vertical Electrical Sounding (VES) methods were employed to evaluate the groundwater potential of University of Ibadan cooperative housing estate in Alabata, Ibadan.

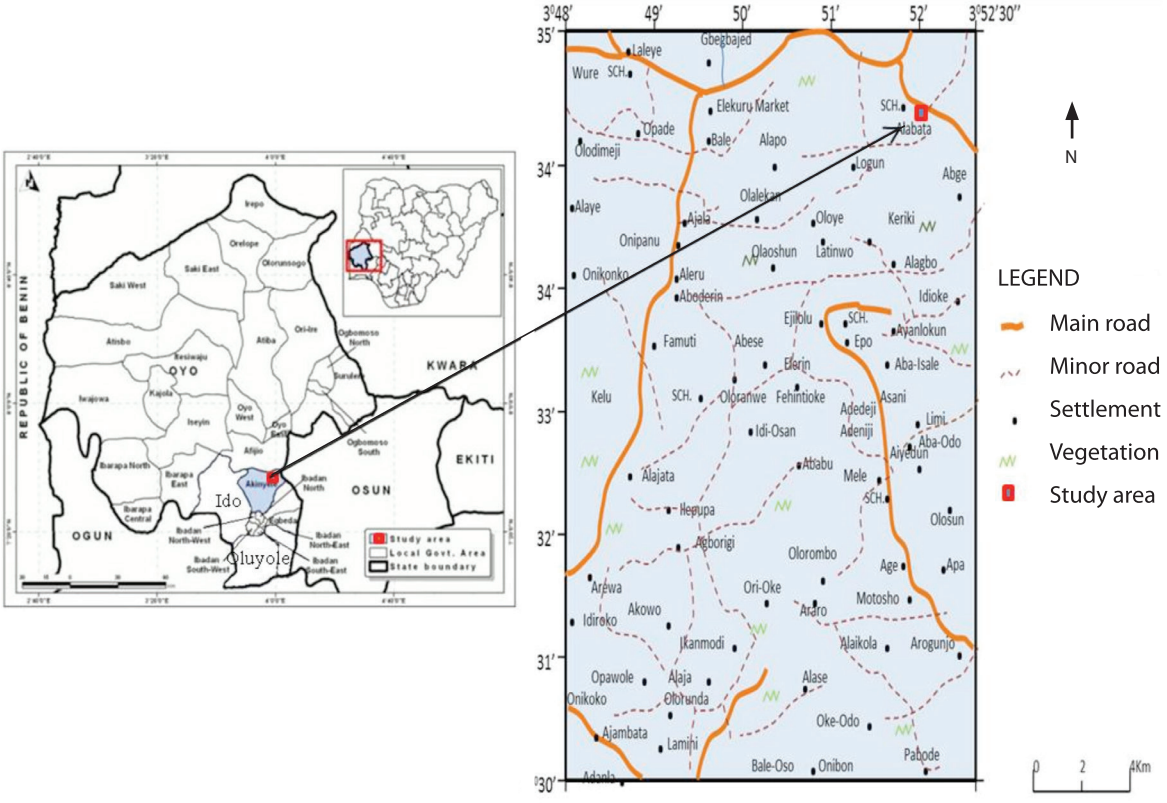

Figure 1: *Location map of the study area.*

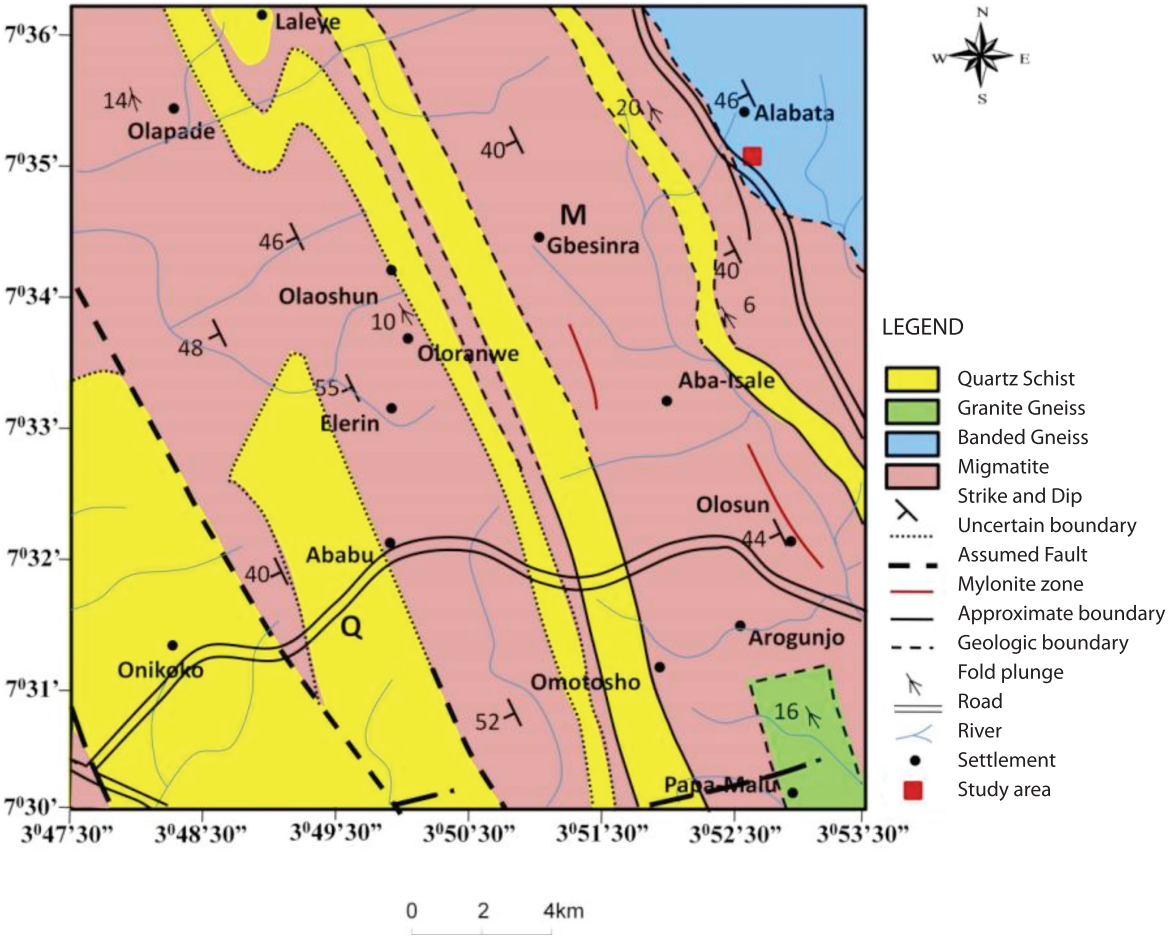

Figure 2: *Geological map of the study area (Afenkhare, 2012).*

Site Description and Geological Setting

The study area is located in Alabata, Ibadan, southwestern Nigeria (Figure 1). It is confined within latitudes 7° 34.970 and 7° 35.138 and longitudes 3° 52.180 and 3° 52.0. The study area is characterized by relatively gentle undulating terrain with elevations of between 265 m and 278 m above mean sea level (msl). The vegetation in the area is of rainforest type, characterized by short dry season and long wet season, with high annual rainfall ranging between 1 000 mm and 1 200 mm. Annual mean temperature is between 22 °C and 33 °C with relatively high humidity.[7] The survey area is underlain by the Precambrian basement complex rock of southwestern Nigeria. Metamorphic basement rocks, mostly undifferentiated migmatite-gneiss, quartzite-schist, banded gneiss and granite gneiss, underlie the area.[8] Figure 2 highlights the local geology of study area. The study area falls in the area underlain by banded gneiss in Alabata. The coarse-grained banded gneiss was low-lying with the elevation ranging from 240 m to 290 m (msl). It strikes approximately north-south with minor folds. There are quartz and pegmatite intrusions occurring concordantly with the rock's strike direction.

Materials and methods

The field investigation involved application of both Very Low Frequency Electromagnetic (VLF-EM) measurements and Vertical Electrical Sounding (VES) for mapping fractures in the bedrock and delineating geoelectrical layers in the overburden materials.

VLF measurement

VLF surveying falls into the far-field system of electromagnetic data collection. The VLF transmitter is a military-based communications antenna that emits a very powerful electro-

magnetic wave, which when detected tens of kilometers from the source, behaves as a horizontally propagated plane wave.[9] The propagating signal has horizontal and linearly polarized magnetic and electrical components of the radio-wave field in the absence of a subsurface conductor. However, eddy currents are generated when the radio-wave field passes through a buried conductor, creating a secondary electromagnetic field. The increase in the flow of induced current causes the magnetic field to tilt in the vicinity of conducting structures.[10] Since this causes a phase shift with respect to the homogeneous primary field, the total field is elliptically polarized and tilts with respect to the horizontal axis. Consequently, tilt-angle variations follow a response across the anomaly and thus the crossover point coincides with the center of the anomaly.

Many commercial instruments measure the changes in the different parameters of the total field. For example, some instruments measure the dip of the major axis and the ellipticity of the polarization ellipse; whereas other instruments measure the vertical and horizontal field components. These components of the anomalous field can be converted into ratios of the vertical anomalous field to the horizontal primary field for tilt angle analysis. Further, a current density can be calculated with respect to depth from the measured magnetic field. For example, a buried sheet conductor in a resistive medium in a horizontal primary magnetic field will induce changes in the amplitude and direction of the primary field in proximity to the target. Consequently, on one side of the target, the angle between the vectors of the primary and secondary components of the radio wave field will reach a maximum near an object and change to a minimum upon passing a buried target. The point at which the tilt angle passes through zero, the "crossover" point lies immediately above the target.[11] If the target dips, then the tilt-angle measurements on one side of the anomaly are accentuated at the expense of the tilt-angle measurements on the other side of the target. The tilt angle and current density derived from the anomalous magnetic field can be used in subsequent statistical analyses to locate and to image the subsurface target.

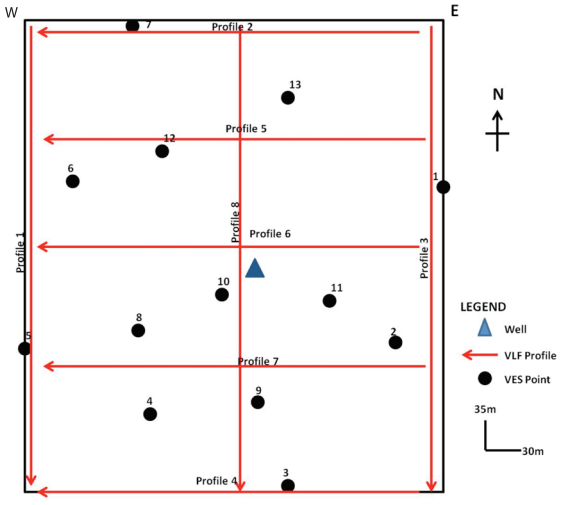

Figure 3: *Location map of the study area showing the VLF-EM profiles, VES points and dug well.*

Linear filtering of the tilt-angle measurements can aid in locating the position of a buried target. Fraser[12] proposed a simple linear statistical filter of tilt-angle data that converts tilt-angle crossovers into peaks for ease of analysis. Fraser filtering consists of averaging the tilt-angle measurement produced by a subsurface conductor. In a linear sequence of tilt-angle data M_1, M_2, M_3 ... M_n measured at a regular interval, the Fraser filter F_i is:

$$\Phi_1 = (M_3 + M_4) - (M_1 - M_2) \quad (1)$$

The first value F_1 is plotted half way between positions M_2 and M_3; the second value is plotted halfway between M_3 and M_4.

Many instruments can calculate a current density from the magnitude of the measured magnetic field.[13] Karous and Hjelt[14] developed a statistical linear filter, based upon[12] and linear field theory of Bendat and Piersol[15] This filter provides an apparent depth profile from the current density (H0) which is derived from the magnitude of the vertical component of the magnetic field at a specific location (Figure 3). The depth profile can be calculated from:

$$I_a(0) = 2\pi\,(-0.102H_{-1} + 0.059H_{-2} - 0.561H_{-1} + \\ + 0.561H_1 - 0.059H_2 + 0.102H_3)/Z \quad (2)$$

Where, the equivalent current density I_a at a specified horizontal position and depth Z is based upon a symmetrical filter of the measured current (from the measured magnetic component of the anomalous field).

In this study, VLF-EM method was employed to map the study area with the object of isolating fracture zones which are likely to be filled with water. ABEM Wadi VLF electromagnetic equipment with in-built digital display unit and powered by battery was used. For the VLF-EM measurements, radio signal from station GQD in Rugby UK was the main signal station tuned / selected. This corresponds to frequency values of 18.8 kHz and was employed to generate the primary electromagnetic field around the buried conductors in order to induce the detected secondary field and measured as a fraction of the primary field by the VLF-meter.

Eight profiles were measured with three (3) trending approximately N–S and five (5) trending approximately E–W with measurement station intervals of 10 m. The profiles ranges between 170 m and 250 m long and the majority of the profiles run perpendicular to the general N–S geologic strike in the study area (Figure 3). A sub-meter-accurate Global Positioning System (GPS) was used for exact spatial positioning of collected data.

Geoelectric resistivity measurement

Electrical resistivity data were acquired using the Campus Ohmega resistivity meter. The survey involved 1-D Vertical Electrical Sounding (VES). The VES utilized the Schlumberger electrode array with half-current electrode separation (AB/2) ranging from 1 m to 100 m and thirteen (13) VES stations were occupied (Figure 3). The coordinates of each VES station were taken with the Garmin handheld Global Positioning System (GPS) device to ensure accurate future geo – referencing

Data Processing and Evaluation

The VLF-EM data as well as those of the VES measurements were subjected to data processing and evaluation as the basis for interpretation.

For VLF-EM, the acquired field data were processed to simplify the obtained complex information into a profile in which the displayed function is directly related to physical property of the underlying rock. Thus, measured raw real and imaginary components were subjected to Fraser[12] and Karous-Hjelt[14] filtering operations to suppress noise and enhance signal. The Fraser filter[12] converts crossover points into peak responses by 90° phase shifting. This process removes direct current bias that reduces the random noise between consecutive stations resulting from very low frequency component of sharp irregular responses.[16] The Karous-Hjelt filter[14] uses the linear fit theory to solve the integral equation for the current density. This forms the basis of the overall interpretation and delineation of potential fracture zone.

The VES, field data were interpreted through the following steps:

- smoothing of the apparent resistivity field data curve and removing the electrical noises superimposed using an appropriate filter operator;[17]
- matching the smoothed field curve with the standard curves of the auxiliary method;[18, 19]
- preparing an initial geo-electrical model (thicknesses and corresponding resistivities) for a limited number of layers and incorporating the geological background and well information in the study area;[6]
- entering the initial geo-electrical model into the Vander Velpen[20] modeling package. Iterations were carried out to reach the best fit between the smoothed field curve and the calculated one. The root mean square (RMS) errors of the resulting models ranged between 2.3 % and 3.2 %. The final VES interpretation results (layer resistivities and thicknesses) were used to generate secondary geoelectric (Dar-Zarrouk) parameters, weathered layer thickness map, weathered layer resistivity map, overburden thickness map, bedrock resistivity map and the basement topography map of University of Ibadan cooperative housing estate in Alabata, Ibadan. The spatial representation of the data was done using surfer 9.0 software with Kriging employed as the gridding method. The data were ranked using the overburden thickness, aquifer resistivity, aquifer thickness and bedrock topography inferred from the first order geoelectric parameters and total longitudinal unit conductance, total transverse resistance unit and electrical anisotropy inferred from second order geoelectric parameter to generate the groundwater potential map of the study area.

Geoelectric (Dar-Zarrouk) Parameters

A geo-electric layer is described by two fundamental parameters: its resistivity (ρ_i) and thickness (h_i), where the subscript i indicates the position of the layer in the section. Other geoelectric parameters can be derived from its resistivity and thickness.[21] For $i = 1, 2 \ldots n$-layer, these parameters are:

— Total longitudinal conductance (S)
$S/\Omega = h_1/\rho_1 + h_2/\rho_2 + \ldots + h_n/\rho_n$

Total transverse resistance (T)
$T/(\Omega\ m^2) = h_1\,\rho_1 + h_2\,\rho_2 + \ldots + h_n\,\rho_n$

Maillet[22] has defined S and T as Dar-Zarrouk parameters. They can be defined for individual layers, or as a summation for a multi-layer section.

— Average longitudinal resistivity (ρ_L)
$\rho_L/(\Omega\ m) = H/S = \Sigma\, h_i/(\Sigma h_i/\rho_i)$

Where $H = \Sigma\, h_i$ (h_i is the thickness for each layer i)

— Average transverse resistivity (ρ_t)
$\rho_t/(\Omega\ m) = T/H = (\Sigma h_i\,\rho_i)/\Sigma h_i$

— Electric anisotropy (λ)
$\lambda = (\rho_t/\rho_L)^{1/2} = (T\,S/H^2)^{1/2}$ (dimensionless)

— Root means square resistivity (ρ_m)
$\rho_m/(\Omega\ m) = (\rho_t \times \rho_L)^{1/2} = \lambda \times \rho_L = (1/\lambda) \times \rho_t$

In this study area, the above geoelectric parameters (S, T, ρ_L and ρ_m) are calculated to the top of the basement rock as shown in Table 1.

Table 1: *Calculated geoelectric (Dar-Zarrouk) parameters*

VES NO	LATITUDE*	LONGITUDE*	Elevation (m)	ℓ_1 (Ω m)	ℓ_2 (Ω m)	ℓ_3 (Ω m)	ℓ_4 (Ω m)	h_1 (m)	h_2 (m)	h_3 (m)	S (1/Ω)	T (Ω m²)	λ	M (m)
1	596129.48	838398.80	278.5	113.8	115.8	1823.6	_	1.7	5.6	_	0.063 3	841.94	1.00	267.3
2	596107.62	838297.41	277.1	221.8	57.2	3643.6	_	1.1	7.3	_	0.132 6	661.54	1.11	259.6
3	596058.17	838199.66	270.6	294.8	740.9	620.5	2 489.9	1.2	7.1	10.8	0.031 1	12 315.55	1.02	248.9
4	595993.71	838252.97	268.3	326.8	53.5	5365.4	_	0.8	4.1	_	0.079 1	480.79	1.26	268.1
5	595936.63	838293.39	264.9	110.6	72.8	1155.4	_	1.1	7.0	_	0.106 1	631.26	1.01	257.9
6	595958.47	838402.14	270.4	440.0	35.4	1146.0	_	2.2	8.3	_	0.239 5	1 261.82	1.66	256.5
7	595987.68	838509.07	272.0	58.0	158.8	37.9	1 906.6	1.8	5.1	11.3	0.361	1 342.55	1.00	247.8
8	595989.92	838509.07	268.3	427.0	46.6	1230.4	_	1.2	6.2	_	0.135 9	801.32	1.44	276.6
9	596045.18	838308.23	269.9	357.9	41.9	739.6	_	1.2	7.0	_	0.170 4	722.78	1.35	263.8
10	596026.65	838260.44	273.2	702.3	51.5	2803.9	_	1.0	6.2	_	0.121 8	1 021.6	1.01	269.8
11	596076.30	838328.58	271.2	153.4	29.0	1813.3	_	1.7	6.1	_	0.221 4	437.68	1.26	267.2
12	595998.88	838422.49	274.8	237.4	57.3	792.4	_	2.0	11.5	_	0.209 1	1 133.75	1.14	264.5
13	596055.81	838457.61	274.0	127.6	148.1	133.3	2 709.9	1.5	10.7	4.2	0.115 5	2 335.93	1.00	263.6

*Date for geographic coordinates is Universal Transverse Mercator (UTM)
$\ell_1 - \ell_4$ = Resistivity values for each layer (Ω m)
$h_1 - h_3$ = True thickness for each layer (m)
S = Total longitudinal conductance (1/Ω) to the top of the basement rock
T = Total transverse resistance (Ω m²)
λ = Electric anisotropy (dimensionless) to the top of the bedrock
M = Bedrock relief (m)

Results and discussion

VLF-EM Survey

Fraser filtering responses ranged in value from –105 % to 160 % along the profiles. Figure 4 shows the Fraser filtered data (real or in-phase components). The in-phase profiles show positive peaks of different intensities and sharpness, suggesting the presence of shallow and deep conductors.[23]

Lower values of relative current density correspond to higher values of resistivity.[24] All the VLF-EM profiles in this study were processed using the Karous–Hjelt filter.[25] Conductors (coloured red) were delineated from equivalent current density pseudo sections along

traverse 1, 3 and 7 (Figure 4). A higher value of relative current density is regarded as conductive subsurface structures, such as fractures,[23, 26] which often store groundwater in hard rock terrains.

The 2-D inversion shows the variation of equivalent current density, and change in conductivity with depth. With such equivalent current density cross-section plots, it is possible to qualitatively discriminate between conductive and resistive structures where a high positive value corresponds to conductive subsurface structure and low negative values are related to resistive materials.[24, 26] In addition, equivalent current density cross-section also gives an idea about the dip direction; however, exact dip angle cannot be estimated due to the vertical axis variable being a pseudo depth only.[26, 27]

The equivalence current density pseudo-section of profile 1 (Figure 4a) reveals the presence of major anomaly at the southern section between 125 m and 162 m, which can be referred to as fracture zone.[28] Furthermore, two high current density zones between 17 m and 26 m, and 75 m along the profile can also be referred to as indications of the potential subsurface fracture system[26] with the fracture at 75 m dipping southwest (Figure 4a). Asymmetry in the observed real and imaginary anomalies suggests the dipping nature of a subsurface conductive body.[29, 30] The Fraser filtering data plots and the Karous-Hiljet current density plot for profile 3 as presented in Figure 4a reveals a number of anomalies, which reflects conductive subsurface structural trends of inferred fractures zones. In addition, profile 7 shows

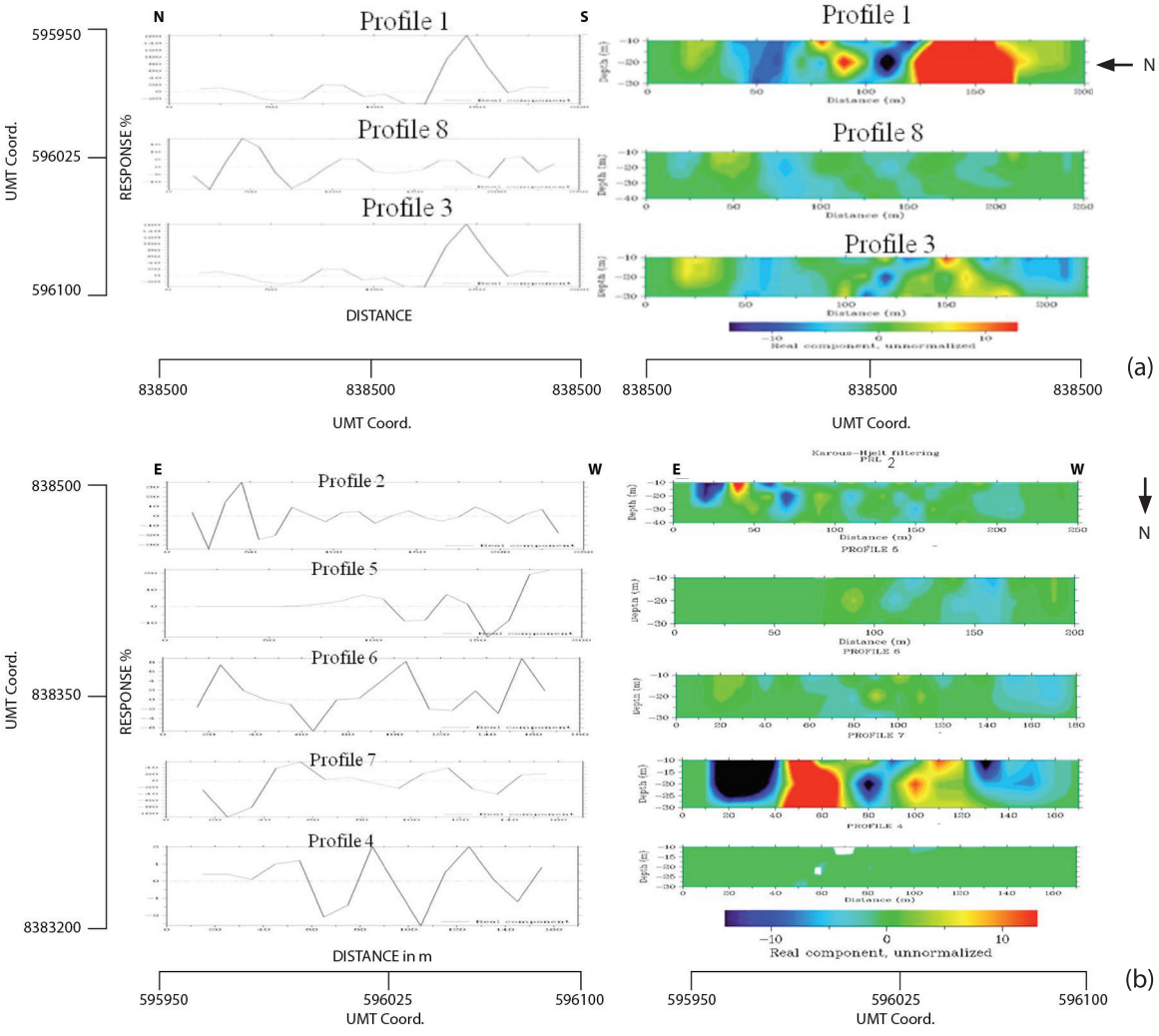

Figure 4: *Fraser filtering graph and equivalent current density pseudo-sections: (a): N-S direction, (b): E-W direction.*

high equivalent current density between stations 42 m and 68 m and station 110 m with the latter dipping southeast. Other closures of conductive bodies are present on different section with each conductive body coinciding with points identified on the profiles as fractures and or geological features (Figures 4a and b).

Resistivity Sounding Curves

The resistivity sounding curves obtained from the study area varied from the 3-layer (A and H types) to 4 layer (KH) with the H type being the predominant. The typical curve types are as shown in Figure 5. Table 1 gives the summary of the VES interpretation. The thickness and characteristics of the aquifer are fairly known due to the well dug in the centre of the study area. The key to success of any geophysical survey is the calibration of the geophysical data with hydro-geological and geological ground truth information; therefore, geoelectric station 10 was purposely located near the well (Figure 3). Measurements from existing well dug in the area reveal lateritic top soil, sandy clay, and basement rock. The depth of the well measured is 6.2 m and the potentiometric surface is at 5.3 m. The depth measurement correlates fairly well with the interpreted values of VES-10 (Figure 5).

Weathered Basement (Aquifer unit) Resistivity Map

The weathered basement resistivity map (Figure 6) shows the resistivity variation within the aquifer units of the study area. The resistivity value range is between 29 Ω m and 621 Ω m; with a mean value of 104 Ω m. The resistivity is least at the centre towards the western part of the study area with values ranging between 29 Ω m and 100 Ω m. The northern part has resistivity values ranging from 100 Ω m to 150 Ω m with the resistivity increasing towards the north. The resistivity also increases toward the south of the study area with the values ranging between 100 Ω m and 620 Ω m (Figure 6). The classification of the groundwater potential of the aquifer units based on resistivity was premised on the findings of Adiat et al.[2] Zones characterized by resistivity value less than 100 Ω m or greater than 400 Ω m was recognized as area of least groundwater prospect. Zones of medium yield

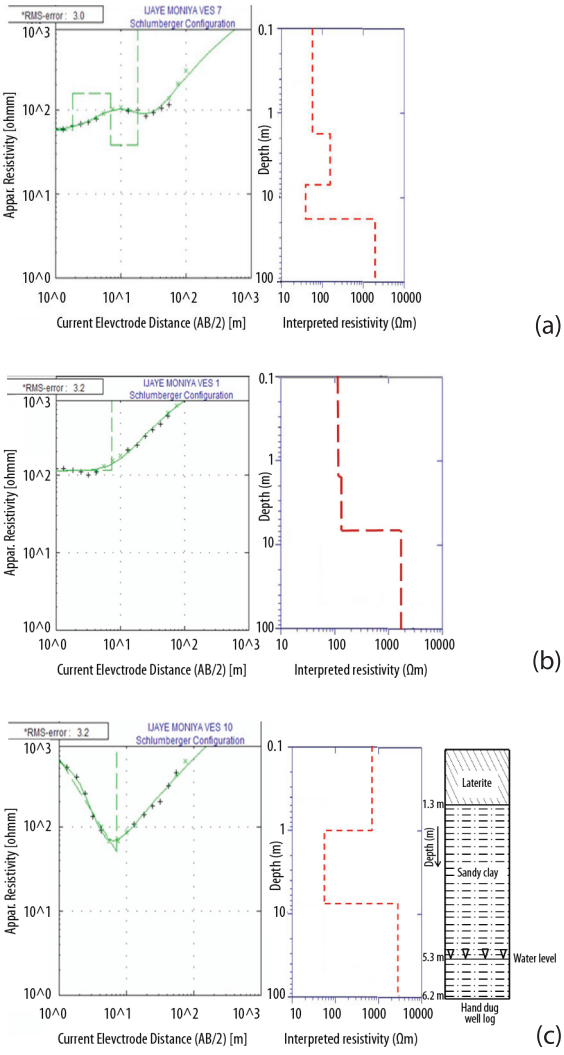

Figure 5: *Representative VES curve in Alabata with their respective interpreted resistivity log. (a): KH curve, (b): A curve & (c): H curve.*

for groundwater prospect are characterized by resistivity values ranging between 300 Ω m to 350 Ω m. Areas with resistivity values between 100 Ω m and 300 Ω m are classified as zones of high groundwater yield potential. In addition, Olayinka et al.[5] classified weathered basement in the basement complex of Nigeria with resistivity values ranging from 100 Ω m to 800 Ω m as good groundwater aquifer. Barker et al.[31] also observed that the highest yielding boreholes in the basement complex of Zimbabwe were associated with weathered layers resistivity values between 100 Ω m and 600 Ω m. Based on these, the northern and southern part of the study area is presumed to have good groundwater aquifer.

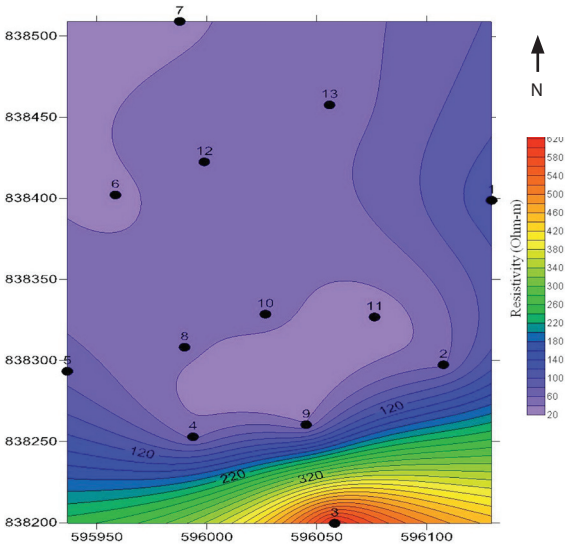

Figure 6: *Aquifer resistivity map of the study area.*

Weathered Basement (Aquifer Unit) Thickness Map

The thickness of the weathered basement varies between 4.1 m and 11.5 m (Table 1). The aquifer unit in the study area has a mean thickness of 7.4 m. The aquiferous zone is relatively thick around the northwest and southeast portion of the study area (8 m to 11.5 m) while the thickness of the remaining part is relatively thin (4.1 m to 8 m) (Figure 7). The aquifer unit in the entire area is generally characterized by low thickness between 4 m to 8 m. However, some areas have relatively thick aquiferous unit with thickness varying between 8 m and 12 m.

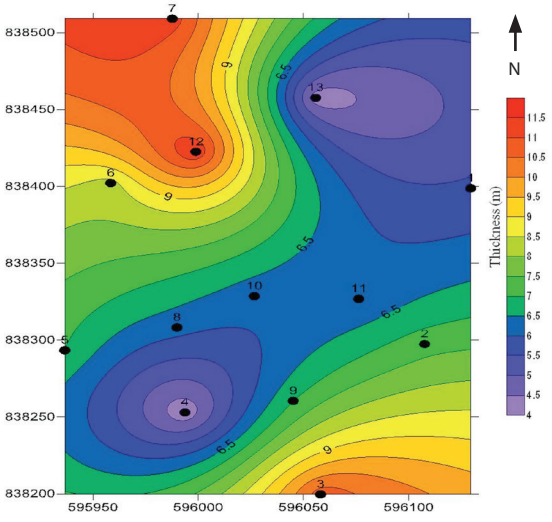

Figure 7: *Aquifer thickness map of the study area.*

Overburden Thickness Map

The overburden thickness map (Figure 8) shows that the overburden thickness of the area varies from 4.9–19.1 m, with a mean of 10.5 m. The overburden thickness map show zones of relatively thick overburden (greater than 13 m) and zone of relatively thin overburden (< 13 m). Appreciable overburden thickness zones are possible groundwater collecting zones; therefore, unconsolidated material could contain reliable aquifer if thick and sandy.[5, 32] Geophysical studies in southwestern basement complex of Nigeria have identified thick overburden as zones of high groundwater potentials.[33–35] The overburden is relatively thick (13 m to 20 m) in the northern and southeastern portions of the study area. These zones are suggestive of possible groundwater potential zones in the area. Such zones cover about 38 % of the entire study area.

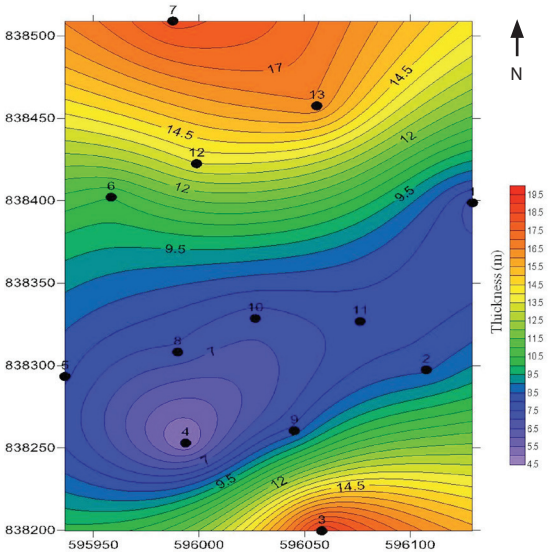

Figure 8: *Overburden thickness map of the study area.*

Aquifer protective capacity evaluation

The total longitudinal conductance (S) to the top of the basement rock ranges between 0.031 1 S and 0.361 S. The maximum value was recorded at VES 7 (0.361 S) with gradual decrease towards the south (Figure 9). The minimum value was recorded at VES 3 (0.031 1 S). A marked increase in *S* may correspond to an average increase in the clay content and consequently a decrease in transmissivity.[6] The total longitudinal unit conductance values can also be utilized in evaluating overburden protective capacity in an

area.[36] This is because the earth medium acts as a natural filter to percolating fluid. Its ability to retard and filter percolating fluid is a measure of its protective capacity.[36, 37] The highly impervious clayey overburden, which is characterized by relatively high conductance, offers protection to the underlying aquifer.[38] The protective capacity of the overburden has been zoned into good, moderate and weak protective capacity.[39] They classified the longitudinal conductance above 0.7 S as good protective capacity zone, the portion having conductance values ranging from 0.2 S to 0.69 S were classified as zone of moderate protective capacity while zone with 0.1 S to 0.19 S was classified as weak protective capacity and where the conductance value is less than 0.1 S were considered poor. The above classification has revealed that the overburden materials of the study area ranging between moderate to poor protective capacity zone. The moderate protective capacity covers the northwestern part of the study area and extends towards the central part, which has weak protective capacity. The northeast through the eastern part to the south of the study area have poor protective overburden (Figure 9). From the longitudinal conductance map of the area, about 30 % of the area falls within the moderate protective capacity while about 70 % constitutes the weak/poor protective capacity rating. This suggests that materials of weak/poor protective capacity underlie the area.

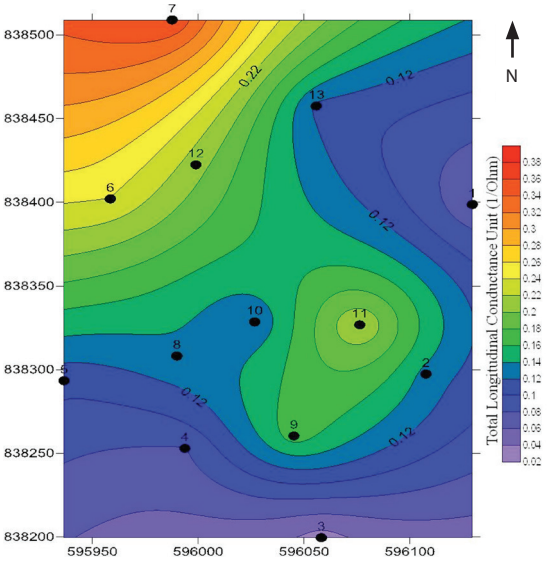

Figure 9: *Total longitudinal conductance unit map of the study area.*

Bedrock Topography Map

The bedrock topography map (Figure 10) reflects the topography of the bedrock underlying the area and its structural disposition. The map shows that the basement structures in the area include both basement ridge and depressions. The ridge occupies the eastern and central parts of the study area while the depressions occupy the northern, western and southern parts of the study area. Naturally, the groundwater flows from areas of high pressure (such as bedrock ridge) to area of low pressure (such as bedrock depression). It is then expected that areas identified as depressions on the map are the groundwater collection points, which have significant role in groundwater development.

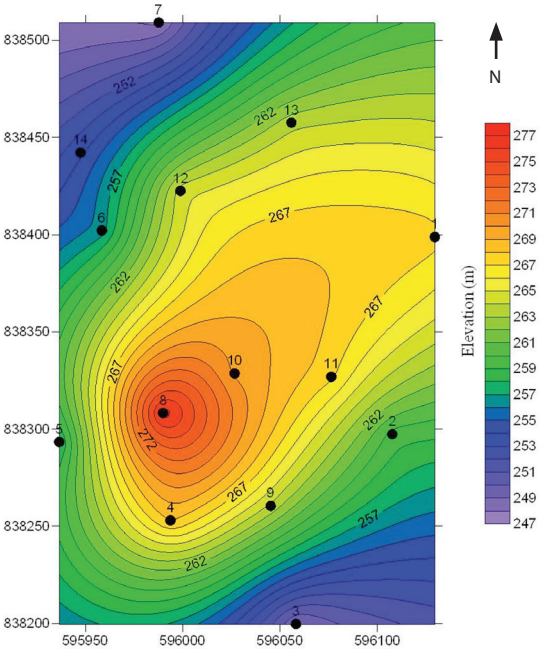

Figure 10: *Bedrock topography map of the study area.*

Electrical anisotropy (λ)

In the study area, the coefficient of anisotropy to the top of the basement rock ranges between 1.00 and 1.66. The maximum λ value was recorded at VES-6 (1.66) and the minimum λ values are recorded at VES-1, 7, and 13 (1.00) (Table 1). The coefficient of anisotropy map (Figure 11) shows that λ is high around the western part of the study area and decreases towards other zones. Singh and Singh[40] pointed out that lower values of anisotropy correspond to high aquifer potential zones. Based on this, the northern portion through the east to

the southern part of the study area is characterized by higher groundwater potential. These areas coincide with the areas with weak/poor protective layers (Figure 9); part of it falls on the ridge in the bedrock topography map (Figure 10), which is the groundwater-diverting zone. This is confirmed by the Fraser filter and equivalent current density distribution in profile 4 (Figure 4b) with high response on Fraser filter graph but with no corresponding accumulation of current density distribution on the equivalent current density pseudo-section. This fracture may contain unsaturated material. However, the depression indicated on the bedrock topography map (Figure 10) contains saturated material presumed to be groundwater as indicated on Fraser filter and equivalent current density pseudo-section of profile 6 (Figure 4b). In addition, the southern part of this area has the requirements that favour groundwater abstraction (Figure 11).

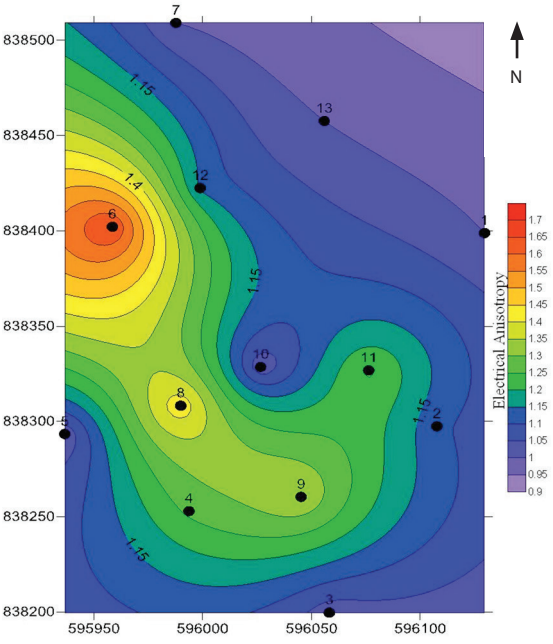

Figure 11: *Electrical Anisotropy map of the study area.*

Bedrock resistivity map

Figure 12 shows the contour map of the bedrock resistivity. The resistivity values of the bedrock vary from 740 Ω m to 5 365 Ω m. According to Olayinka and Olorunfemi,[41] the resistivity values that exceed 1 000 Ω m is fresh bedrock but where the resistivity reduces to less than 1 000 Ω m, the bedrock is fractured

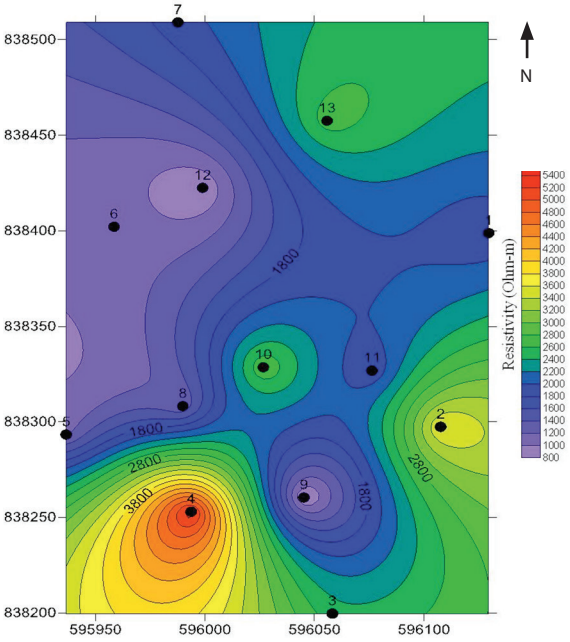

Figure 12: *Bedrock resistivity map of the study area.*

and saturated with fresh water. The fractured zone constitutes a major component of the aquifer in a basement complex area. From the map (Figure 12), the bedrock in the southwestern, southeastern, northeastern and around the central parts is highly resistive (2 000 Ω m to 5 400 Ω m). This coincides with the low conductivity values displayed on the equivalent current density pseudo-section of profiles 1, 2, 5, 7 and 8, which confirms the presence of highly resistive features in those zones. The resistivity values for the bedrock in the northwest to the major parts of the central portion towards the south central ranges between 1 200 Ω m to 2 000 Ω m. There is good correlation between bedrock resistivity map and the equivalent current density pseudo-sections crossing this area, which show shallow conductive features. The resistivity value of the western and minute portion of south central is less than 1 000 Ω m (700 Ω m to 1 000 Ω m). This is revealed by the current density pseudo-sections of profile 1, which shows a highly conductive feature between stations 122 m and 167 m, and profile 7, which has high current density reflection at station 110 m with the fracture dipping southeast. The prominent current density reflects the presence of localized fractures containing groundwater.[26] There is good correlation between the equivalent current density pseudo-sections and the bedrock resistivity map.

Total transverse resistance unit

The total transverse resistance unit (*T*) to the top of the basement rock ranges between 12 315.55 and 437.68 Ω m^2. The maximum *T* value was recorded at VES-3(12 315.55 Ω m^2) with gradual decrease towards the central part. The minimum *T* value was recorded at VES-11 (437.68 Ω m^2) Figure 13 shows the map of total transverse conductance unit of the study area. The southern part has the highest value, which ranging from 1 000 Ω m^2 to 12 300 Ω m^2. The central part has value ranging between 400 Ω m^2 to 1 000 Ω m^2 while the northern zone has value ranges from 1 000 Ω m^2 to 2 500 Ω m^2. Transverse resistance unit map has been used in determination of zones with high groundwater potential.[42] According to Braga et al.[43] high values of *T* can be associated with the zones of high transmissivity and areas with high values on *T* map indicate unconfined aquifer. Hence, the southern zone is suitable for groundwater exploitation.

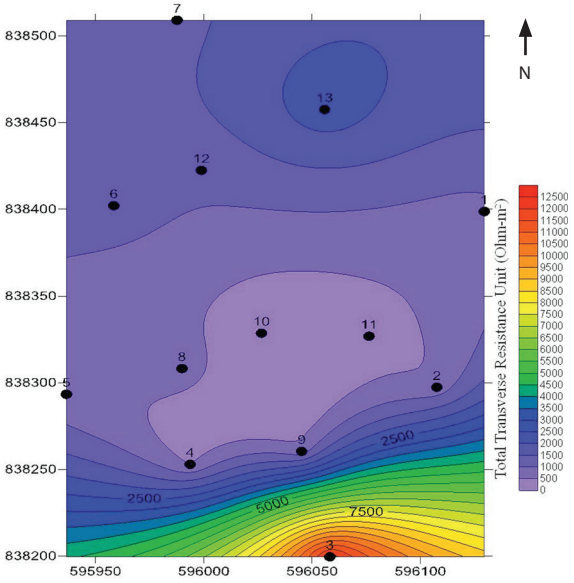

Figure 13: *Total transverse resistance unit map of the study area.*

Groundwater Potential Evaluation

The groundwater potential evaluation of the area was based on the integration of the equivalent current density pseudo-sections, aquifer resistivity, aquifer thickness, overburden thickness, total longitudinal conductance unit, total transverse resistance unit, and electric anisotropy and bedrock topography maps. The groundwater prolific area will have high accumulation of current density, which reflects the presence of fracture zones,[26] thick overburden > 10 m[5] and aquifer resistivity ranging from 100 Ω m to 800 Ω m.[2, 5, 31] In addition, groundwater potential area should have low longitudinal conductance unit, which indicate an increase in transmissivity,[6] high transverse resistance unit,[43] low values of electrical anisotropy < 1.2[40] and areas characterized by depressions on the basement topography map. These maps were synthesized and integrated for the evolvement of the groundwater potential map, which was eventually used to categorize the study area into good, moderate and poor groundwater potential zones (Figure 4). The central/western portion is characterised by decrease in overburden thickness (7.2 m at VES 10), weathered layer resistivity (35 Ω m at VES 6), total transverse resistance unit (723 Ω m^2 at VES 9) and increase in electric anisotropy (1.66 at VES 6) and total longitudinal conductance (0.24 S at VES 6), reflecting low aquifer potential. On the other hand, northeastern/southeastern region is characterized by increase in overburden thickness (19.1 m at VES-3), weathered layer resistivity (602 Ω m at VES-3), total transverse resistance unit (12 316 Ω m^2 at VES 3) and decrease in electrical anisotropy (1.00 at VES-1, 7 and 13) and total longitudinal conductance unit (0.031 1 S at VES-3), reflecting high aquifer potentials. In this regard, the northern and south-eastern parts of the study area are

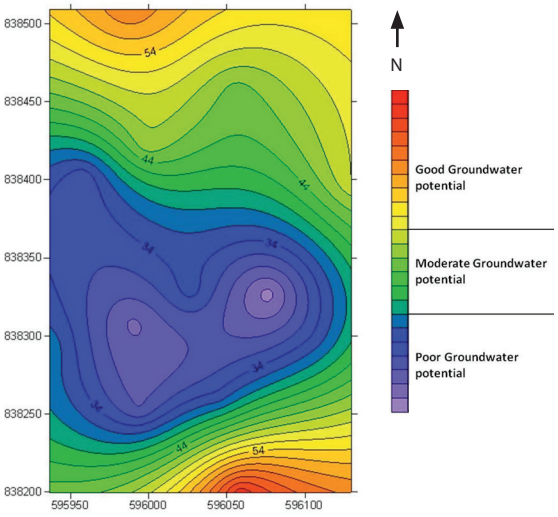

Figure 14: *Groundwater potential map of the study area.*

categorised as good groundwater potential; moving towards the central from the northern and southern parts, groundwater potentiality changes from good to moderate while the western/central part is categorised as area with poor groundwater potential (Figure 14).

Conclusions

A comparative integrated interpretation of VLF-EM and VES data enabled the evaluation of the groundwater prospect of University of Ibadan cooperative housing estate in Alabata, Ibadan; a basement complex terrain of south-western Nigeria. With the additional information obtained from existing well in the area, the spatial distribution of the regolith/weathered layer, containing the near-surface or overburden aquifers, was reliably delineated from the bedrock housing the bedrock aquifers. The geoelectric parameters (layer resistivities and thicknesses) which are known to be of hydrogeologic relevance, gathered from the VES interpretation were used to generate maps (weathered/fractured layer resistivity map, weathered/fractured layer thickness map, overburden thickness map, basement topography map and Dar Zarrouk parameters maps). The maps were interpreted individually by identifying geoelectric parameters favourable to groundwater occurrence. The maps were combined to form a composite entity from which the groundwater potential of the study area was evaluated. The groundwater potential map was used to classify the study area into good, moderate and poor groundwater zones. The hydrogeologic importance of the equivalent current density pseudo-sections, the basement depressions identified on the basement topography map, maps generated from the primary and secondary (Dar Zarrouk) parameters corroborated the deductions from the groundwater map. Zones identified to have moderate and good groundwater potential can be considered for groundwater development at University of Ibadan cooperative housing estate in Alabata, Ibadan. The southern/northern portion was considered as good groundwater prospect area.

Acknowledgements

The authors acknowledged Mr. Isaac O. Babatunde with profound appreciation for the assistance during all the data acquisition. Sincere thanks are given to the anonymous reviewers.

References

[1] Wright, C. P. (1992): The hydrogeology of crystalline basement aquifers in Africa. In: C. P. Wright and W. C. Burgess (eds). Hydrogeology of crystalline basement aquifer in Africa. *Geological Society of London Special Publication*, 66, pp. 1–27.

[2] Adiat, K. A. N., Olayanju, G. M., Omosuyi, G. O. and Ako, B. D. (2009): Electromagnetic profiling and electrical resistivity soundings in groundwater investigation of a typical basement complex-A case of Oda town, southwestern Nigeria. *Ozean Journal of Social Sciences*, 2(4), pp. 333–359.

[3] Flathe, H. (1955): Possibilities and limitations in applying geoelectrical methods to hydrogeological problems in the coastal area of North West Germany. *Geophysical Prospecting*, 3, pp. 95–110.

[4] Zohdy, A. A. R. (1969): The use of Schlumberger and Equatorial soundings in groundwater investigations near El Paso, Texas. *Geophysics*, 34, pp. 713–728.

[5] Olayinka, A. I., Amidu, S. A. and Oladunjoye, M. A. (2004): Use of electromagnetic profiling and resistivity sounding for groundwater exploration in the crystalline basement area of Igbeti, southwestern Nigeria. *Global Journal of Geological Sciences*, 2(2), pp. 243–253.

[6] Khali, M. H. (2009): Hydrogeophysical assessment of Wdi El-Sheikh aquifer, Saint Katherine, South Sinai, Egypt. *Journal of Environmental and Engineering Geophysics*, 14(2), pp. 77–86.

[7] NIMET, (2011): Nigerian Metrological Agency, daily weather guide, Nigeria Television Authority, Lagos, Nigeria.

[8] Afenkhare, E. (2012): *Effects of geologic structures on groundwater in Alabata, southwestern Nigeria.* Unpublished BSc Dissertation, Department of Geology, University of Ibadan B. Sc. project, p. 22.

[9] Nabighian, M. N. and Macae, J. C. (1991): Time domain electromagnetic prospecting methods. In: Nabighian, M. N. (ed.). *Electromagnetic methods in applied geophysics*, 2: Applications, Part B. Tusla, Society of Exploration Geophysicists, pp. 427–520.

[10] McNeill, J. D. (1988): *Electromagnetics: In proceedings on the application of geophysics to engineering and environmental problems*, pp. 251–348.

[11] Babu, E. A., Ram, S. and Sundararajan, N. (2007): Modeling and inversion of magnetic and VLF-EM data with an application to basement fracture- A case study from Raigarh, India. *Geophysics*, 72, p. 133.

[12] Fraser, D. C. (1969): Contouring of VLF-EM data. *Geophysics*, 34, pp. 958–967.

[13] Reynolds, J. M. (1987): *An introduction to applied and environmental geophysics.* Published by John Wiley and Sons Ltd. Baffins lane, Chichester west, Sussex P O 191UD England, p. 796

[14] Karous, M. and Hjelt, S. E. (1983): Linear filtering of VLF dip-angle measurements. *Geophysical Prospecting*, 31, pp. 782–894.

[15] Bendat, J. S. and Piersol, A.G. (1968*): Measurement and analysis of random data, Wiley*, New York.

[16] Al-Tarazi, E., Abu Rajab, J., Al-Naga, A. and El- Waheidi, M. (2008): Detecting leachate plumes and groundwater pollution at Ruseifa municipal landfill utilizing VLF-EM method. *Journal of Applied Geophysics*, 62, pp. 121–131.

[17] Ghosh, D. P. (1971): The application of linear filter theory to the direct interpretation of geoelectric resistivity soundings measurements. *Geophysical Prospecting*, 19(2), pp. 192–217.

[18] Mooney, H. M, Orellana, E., Pickett, H., Tornhein, L. (1960): A resistivity computation method for layered earth models. *Geophysical Prospecting*, 31, pp. 192–203.

[19] Marsden, D. (1973): The automatic fitting of a resistivity sounding by a geometric progression of depth. *Geophysical Prospecting*, 21, pp. 266–280.

[20] Vander Velpen, B. P. A. (1988): Resist software version 1.0: M.Sc. research project ITC, Delft, Netherlands. Copyright@2004, ITC, IT-RSG/DSG.

[21] Zohdy, A. A. R., Eaton, G. P., Mabey, D. R. (1974): *Application of surface geophysics to groundwater investigations.* In Tech. of Water Sources Investigations of the U.S. Geol. Survey, Book 2, Chap. D1.

[22] Maillet, R. (1974): The fundamental equations of electrical prospecting. *Geophysics*, 12, pp. 529–556.

[23] Santos, F. A. M., Mateus, A., Figuerias, J. and Gondres, M. A. (2006): Mapping groundwater contamination around a landfill facility using the VLF-EM method- A case study. *Journal of Applied Geophysics*, 60, pp. 115–125.

[24] Benson, A. K., Payne, K. L. and Stubben, M. A. (1997): Mapping groundwater contamination using DC resistivity and VLF geophysical methods-a case study. *Geophysics*, 62, pp. 80–86.

[25] Pirttijärvi, M. (2004): Karous–Hjelt and Fraser filtering of VLF measurements. Manual of the KHFFILT Program.

[26] Sharma, S. P. and Baranwal, V. C. (2005): Delineation of groundwater-bearing fracture zone in a hard rock area integrating Very Low Frequency electromagnetic and resistivity data. *Journal of Applied Geophysics*, 57, pp. 155–166.

[27] Adelusi, A. O., Adiat, K. A. N. and Amigun, J. O. (2009): Integration of surface electrical prospecting methods for fracture detection in Precambrian basement rocks of Iwaraja area, southwestern Nigeria. *Journal of Applied Sciences*, 2(3), pp. 265–280.

[28] Tijani, M. N., Osinowo, O. O. and Ogedengbe, O. (2009): Mapping subsurface fracture systems using integrated electrical resistivity profiling and VLF-EM methods: a case study of suspected gold mineralization. *RMZ- Materials and Geoenvironment*, 56(4), pp. 415–436.

[29] Ogilvy, R. D. and Lee, A. C. (1991): Interpretation of VLF-EM in phase data using current density pseudo-sections. *Geophysical Prospecting*, 39, pp. 567–580.

[30] Kaikkonen, P. and Sharma, S. P. (1998): 2-D nonlinear joint inversion of VLF and VLF-R data using simulating annealing. *Journal of Applied Geophysics*, 39, pp. 155–176.

[31] Barker, R. D., White, C. C. and Houston, D. F. (1992): Borehole siting in an African Accelerated Drought Relief Project. Hydrogeology of crystalline basement aquifers in Africa. *Geological Society of London special publication*, 66, pp. 183–201.

[32] Satpathy, B. N. and Kanungo, B. N. (1976): Groundwater exploration in hard rock, a case study. *Geophysical Prospecting*, 24(4), pp. 725–736.

[33] Olorunfemi, M. O. and Okhue, E. T. (1992): Hydrogeological and Geologic significance of a geoelectric survey at Ile-Ife. *Nigeria Journal of Mining and Geosciences Society*, 28, pp. 221–229.

[34] Oladapo, M. I., Mohammed, M. Z, Adeoye, O. O. and Adetola, B. A. (2004): Geoelectric investigation of the Ondo state housing corporation estate, Ijapo Akure, southwestern Nigeria, *Journal of Mining and Geology*, 40(1), pp. 41–48.

[35] Oyedele, E. A. and Olayinka, A. I. (2012): Statistical evaluation of groundwater potential of Ado-Ekiti southwestern Nigeria. *Transnational Journal of Science and Technology*, 2(6), pp. 110–127.

[36] Abiola, O., Enikanselu, P. A. and Oladapo, M. I. (2009): Groundwater potential and aquifer protective capacity of overburden units in Ado-Ekiti, Southwestern Nigeria. *International Journal of the Physical Sciences*, 5(5), pp. 415–420.

[37] Olorunfemi, M. O., Ojo, J. S. and Akintunde, O. M. (1999): Hydrogeophysical evaluation of the groundwater potential of Akure metropolis, southwestern Nigeria. *Journal of Mining and Geology*, 35(2), pp. 207–228.

[38] Ariyo, S. O. and Adeyemi, G. O. (2011): Integrated geophysical approach for groundwater exploration in hard rock terrain-A case study from Akaka area of southwestern Nigeria. *International Journal of Advanced Scientific and Technical Research*, 2(1), pp. 376–395.

[39] Oladapo, M. I. and Akintorinwa, O. J. (2007): Hydrogeophysical study of Ogbese, southwestern Nigeria. *Global Journal of Pure and Applied Science*, 13(1), pp. 55–61.

[40] Singh, C. L. and Singh, S. N. (1970): Some geo-electrical investigations for potential groundwater in part of Azamgraph area of U.P. *Journal of Pure and Applied Geophysics*, 82, pp. 270–285.

[41] Olayinka, A. I. and Olorunfemi, M. O. (1992): Determination of geo-electrical characteristics in Okene area and implications for borehole siting. *Journal of Mining and Geology*, 28(2), pp. 403–412.

[42] Nafez, H., Kaita, H. and Samer, F. (2010): Calculation of transverse resistance to correct aquifers resistivity of groundwater saturated zones: Implication for estimated its hydrogeological properties. *Lebanese Science Journal*, 11(1), pp. 105–115.

[43] Braga, O. C., Filho, W. M. and Dourado, J. C. (2006): Resistivity (DC) method applied to aquifer protection studies. *Brazilian Journal of Geophysics*, 24(4), pp. 574–581.